EARTHQUAKE ENGINEERING AND STRUCTURAL DYNAMICS
Earthquake Engng Struct. Dyn. 2003; **32**:187–206 (DOI: 10.1002/eqe.219)

A neural network approach for structural identification and diagnosis of a building from seismic response data

C. S. Huang*,†, S. L. Hung, C. M. Wen and T. T. Tu

Department of Civil Engineering, National Chiao Tung University, Hsinchu 30050, Taiwan

SUMMARY

This work presents a novel procedure for identifying the dynamic characteristics of a building and diagnosing whether the building has been damaged by earthquakes, using a back-propagation neural network approach. The dynamic characteristics are directly evaluated from the weighting matrices of the neural network trained by observed acceleration responses and input base excitations. Whether the building is damaged under a large earthquake is assessed by comparing the modal parameters and responses for this large earthquake with those for a small earthquake that has not caused this building any damage. The feasibility of the approach is demonstrated through processing the dynamic responses of a five-storey steel frame, subjected to different strengths of the Kobe earthquake, in shaking table tests. Copyright © 2002 John Wiley & Sons, Ltd.

KEY WORDS: system identification; damage assessment; neural network; earthquake responses

1. INTRODUCTION

A structure may sustain damage either when subjected to severe loading like a strong earthquake or when its material deteriorates. Damage is traditionally assessed by visual inspection, which is costly and inefficient. Various innovative sensor technologies have recently been developed and applied to monitor buildings and infrastructure. It is desirable to use the measured data to determine whether a structure is damaged and, further, the nature of any such damage.

The damage of a structure is conventionally assessed from observed dynamic responses by detecting changes in the modal parameters of the structure. The concept underlying such an

*Correspondence to: C. S. Huang, Department of Civil Engineering, National Chiao Tung University, 1001 Ta-Hsueh Road, Hsinchu 30050, Taiwan.
†E-mail: cshuang@cc.nctu.edu.tw

Contract/grant sponsor: National Science Council, R.O.C.; contract/grant number: NSC-90-2211-E-009-031.

Received 10 November 2001
Revised 25 April 2002
Accepted 8 May 2002

approach is that damage to a structure reduces its natural frequencies, increases the modal damping, and changes the modal shapes. Hearn and Testa [1] applied a perturbation method to process measured dynamic responses of a steel frame in a laboratory, and found that changes in natural frequencies and modal damping are good indices for damage. However, from dynamic tests on bridges, Alampalli and Fu [2] and Salawu and Williams [3] concluded that the change in natural frequencies is not sufficiently sensitive to detect local damage in the structure. The results of Salawu and Williams [3] indicate that the modal assurance criterion (MAC) and the co-ordinate modal assurance criterion (CMAC) are useful in detecting local structural change. Using modal parameters, Koh *et al.* [4] proposed an improved-condensation method to estimate the stiffness matrix that corresponds to observed degrees of freedom. Then, these authors detected local structural changes by quantifying changes in stiffness.

Over the last two decades, artificial neural networks (ANN) have gradually been established as a powerful tool in pattern recognition, signal processing, control and complex mapping problems, because of their excellent learning capacity and their high tolerance to partially inaccurate data. Artificial neural networks have, recently, been further applied to assess damage in structures. Wu *et al.* [5] used a back-propagation neural network (BPN) to elucidate damage states in a three-storey frame by numerical simulation. The Fourier spectra of the acceleration responses and the stiffness of members were, respectively, used in the input and output layers of the neural network. Elkordy *et al.* [6] used a back-propagation neural network with modal shapes in the input layer, to detect the simulated damage of structures. Szewczyk and Hajela [7] applied an improved counter-propagation neural network to evaluate a reduction in the member stiffness of a frame structure with nine bending elements, by using measured static displacements under prescribed loads. Pandey and Barai [8] detected damage in a bridge truss by applying ANN of multilayer perceptron architectures to numerically simulated data. Using static displacements, natural frequencies and modal shapes, Zhao *et al.* [9] applied a counter-propagation neural network to locate damage in beams and frames. Masri *et al.* [10] established a method for detecting damage, based on non-linear system identification, in which measured displacement, velocity, acceleration responses and input forces were used to train a back-propagation neural network.

As the first stage of structural damage assessment, this study employed a BPN to diagnose whether a building is damaged by detecting changes in its modal parameters and the dynamic responses in earthquakes. Such work has not yet been discussed in published literature. Only the measured acceleration responses and input base excitations are used to train the neural network. A procedure is also proposed for determining the dynamic characteristics (natural frequencies, modal damping and modal shapes) of the system from trained neural networks. Modal parameters are first employed to diagnose the global changes to the building in earthquakes. Moreover, the trained ANN, based on measured data from the building without any damage in a small earthquake, is employed to predict the responses of the structure under other earthquakes. The considerable differences between the predicted and measured responses further indicate that damage occurred in the building. The dynamic responses of a five-storey steel frame, subjected to various strengths of the Kobe earthquake in shaking table tests, are processed to demonstrate the applicability of the proposed method. The steel frame was shaken to yield in a large magnitude earthquake.

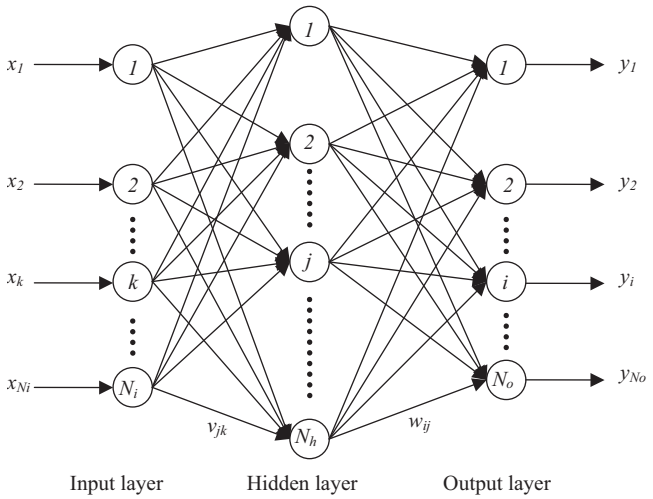

Figure 1. A typical three-layer neural network.

2. ARTIFICIAL NEURAL NETWORK

An ANN model is a system with inputs and outputs based on biological nerves. The system can be composed of many computational elements that operate in parallel and are arranged in patterns similar to biological neural nets. A neural network is typically characterized by its computational elements, its network topology and the learning algorithm used. Among the several different types of ANN, the feedforward, multilayered, supervised neural network with the error backpropagation algorithm—the BPN [11]—is by far the most frequently applied neural network learning model, due to its simplicity.

The architecture of BP networks, depicted in Figure 1, includes an input layer, one or more hidden layers, and an output layer. The nodes in each layer are connected to each node in the adjacent layer. Notably, Hecht–Nielsen [12] proved that one hidden layer of neurons suffices to model any solution surface of practical interest. Hence, a network with only one hidden layer is considered in this study. Before an ANN can be used, it must be trained from an existing training set of pairs of input–output elements. The training of a supervised neural network using a BP learning algorithm normally involves three stages. The first stage is the data feed forward. The computed output of the ith node in output layer is defined as follows:

$$y_i = g\left(\sum_{j=1}^{N_h}(w_{ij}g\left(\sum_{k=1}^{N_i} v_{jk}x_k + \theta_{vj}\right) + \theta_{wi})\right), \quad i = 1,2,\ldots,N_o \tag{1}$$

where w_{ij} is the connective weight between nodes in the hidden layer and those in the output layer; v_{jk} is the connective weight between nodes in the input layer and those in the hidden layer; θ_{wi} (or θ_{vj}) are bias terms that represent the threshold of the transfer function g, and x_k is the input of the kth node in the input layer. Terms N_i, N_h, and N_o are the number of nodes in input, hidden, and output layers, respectively. The transfer function can be linear or non-linear.

The second stage is error BP through the network. During training, a system error function is used to monitor the performance of the network. This function is often defined as follows:

$$E(\mathbf{W}) = \frac{1}{2P}\sum_{p=1}^{P}(\tilde{\mathbf{Y}}_p - \mathbf{Y}_p)(\tilde{\mathbf{Y}}_p - \mathbf{Y}_p)^{\mathrm{T}} \tag{2}$$

where $\tilde{\mathbf{Y}} = (\tilde{y}_1 \tilde{y}_2 \cdots \tilde{y}_i \cdots \tilde{y}_{N_o})$; $\mathbf{Y} = (y_1 y_2 \cdots y_i \cdots y_{N_o})$; $\tilde{y}_i$ is the desired (or measured) value of output node i, and $\mathbf{W} = (v_{11} v_{12} \cdots v_{jk} \cdots v_{N_h} N_i \theta_{v1} \theta_{v2} \cdots \theta_v N_h w_{11} w_{12} \cdots w_{ij} \cdots \; . \; w_{N_o} N_h \theta_{w1} \theta_{w2} \cdots \theta_{wN_o})$.

The final stage is the adjustment of the weights. The standard BP algorithm uses a gradient descent approach with a constant step length (learning ratio) to train the network.

$$\mathbf{W}^{(k+1)} = \mathbf{W}^{(k)} + \Delta\mathbf{W}^{(k)} \tag{3}$$

$$\Delta\mathbf{W}^{(k)} = -\eta\frac{\partial E}{\partial \mathbf{W}^{(k)}} \tag{4}$$

where η is the constant, general learning ratio in the range, $[0, 1]$. The superscript index (k), indicates the kth learning iteration. BP supervised neural network learning models, however, always take an extended period to learn. Moreover, the convergence of a BP neural network is strongly depends upon the use of a learning rate (η). Herein, a more effective adaptive L-BFGS learning algorithm, [13] based on the limited memory Broyden–Fletcher–Goldfarb–Shanno (BFGS) [14] quasi Newton second-order method, with an inexact line search algorithm, is employed. In the conventional BFGS method, the approximation, $\mathbf{H}_{k+1}$, to the inverse Hessian matrix of the error function, E, is updated by

$$\begin{aligned}\mathbf{H}_{k+1} &= (\mathbf{I} - \boldsymbol{\rho}_k \mathbf{s}_k \mathbf{z}_k^{\mathrm{T}})\mathbf{H}_k(\mathbf{I} - \boldsymbol{\rho}_k \mathbf{z}_k \mathbf{s}_k^{\mathrm{T}}) + \boldsymbol{\rho}_k \mathbf{s}_k \mathbf{s}_k^{\mathrm{T}} \\ &\equiv \mathbf{V}_k^{\mathrm{T}} \mathbf{H}_k \mathbf{V}_k + \boldsymbol{\rho}_k \mathbf{s}_k \mathbf{s}_k^{\mathrm{T}}\end{aligned} \tag{5}$$

where

$$\boldsymbol{\rho}_k = 1/\mathbf{z}_k^{\mathrm{T}} \mathbf{s}_k \tag{6}$$

$$\mathbf{V}_k = \mathbf{I} - \boldsymbol{\rho}_k \mathbf{z}_k \mathbf{s}_k^{\mathrm{T}} \tag{7}$$

$$\mathbf{s}_k = \mathbf{W}^{(k+1)} - \mathbf{W}^{(k)} \tag{8}$$

$$\mathbf{z}_k = \mathbf{g}_{k+1} - \mathbf{g}_k \tag{9}$$

and

$$\mathbf{g}_k = \frac{\partial E}{\partial \mathbf{W}^{(k)}} \tag{10}$$

Rather than forming the matrix $\mathbf{H}_k$ in the BFGS method, the vectors $\mathbf{s}_k$ and $\mathbf{y}_k$ first define and then implicitly and dynamically update the Hessian approximation using information from the

preceding few iterations. Therefore, the final stage of adjusting weights in a supervised ANN is modified as follows:

$$\mathbf{W}^{(k+1)} = \mathbf{W}^{(k)} + \alpha_k \mathbf{d}_k \tag{11}$$

The search direction is given by

$$\mathbf{d}_k = -\mathbf{H}_k \mathbf{g}_k + \beta_k \mathbf{d}_{k-1} \tag{12}$$

where

$$\beta_k = \frac{\mathbf{z}_{(k-1)}^{\mathrm{T}} \mathbf{H}_{(k-1)} \mathbf{g}_{(k-1)}}{\mathbf{z}_{(k-1)}^{\mathrm{T}} \mathbf{d}_{(k-1)}} \tag{13}$$

The step length, α_k, is mathematically adapted during the learning process, according to the inexact line search algorithm. This algorithm is used rather than a constant learning ratio in the L-BFGS learning algorithm [13]. It is based on three sequential operations bracketing, sectioning, and interpolation. The bracketing operation brackets the potential step length, α, between two points, through a series of function evaluations. Sectioning then takes the two points of the bracket, for example α_1 and α_2, as the initial points, reduces the step size piecemeal, and determines the minimum between the points, to a desired degree of accuracy. Finally, quadratic interpolation approach takes the three points, α_1, α_2, and $(\alpha_1 + \alpha_2)/2$, to fit a parabola and thus determine the step length, α_k. Accordingly, the step length, α_k, must satisfy the following conditions in each iteration [13]:

$$E(\mathbf{W}^{(k)} + \alpha_k \mathbf{d}_k) \leqslant E(\mathbf{W}^{(k)}) + \beta \alpha_k (\nabla E(\mathbf{W}^{(k)})^{\mathrm{T}} \mathbf{d}_k) \quad \beta \in (0,1) \text{ and } \alpha_k > 0 \tag{14}$$

$$\nabla E(\mathbf{W}^{(k)} + \alpha_k \mathbf{d}_k)^{\mathrm{T}} \mathbf{d}_k \geqslant \theta (\nabla E(\mathbf{W}^{(k)})^{\mathrm{T}} \mathbf{d}_k \quad \theta \in (\beta, 1) \text{ and } \alpha_k > 0 \tag{15}$$

$$\nabla E(\mathbf{W}^{(k)} + \alpha_k \mathbf{d}_k)^{\mathrm{T}} \mathbf{d}_{(k+1)} < 0 \tag{16}$$

Hence, the problem of trial and error selection of a learning ratio in the conventional BP algorithm is avoided in the adaptive L-BFGS learning algorithm.

3. STRATEGY FOR DAMAGE DIAGNOSIS

The basic concept behind the proposed methodology is that a structural system behaves linearly in small earthquakes that may frequently occur in seismically active areas. The structural system, however, may experience varying degrees of damage in large earthquakes, exhibiting non-linear behaviour. Thus, training an ANN to represent faithfully the linear responses of the undamaged system, using the responses observed in small earthquakes, yields notable prediction errors for the non-linear responses. In real applications, damage in secondary structural components may also cause such a prediction error. However, modal parameters are good indices for confirming damage in primary structural components. Damage to secondary structural components does not typically, significantly change the modal parameters.

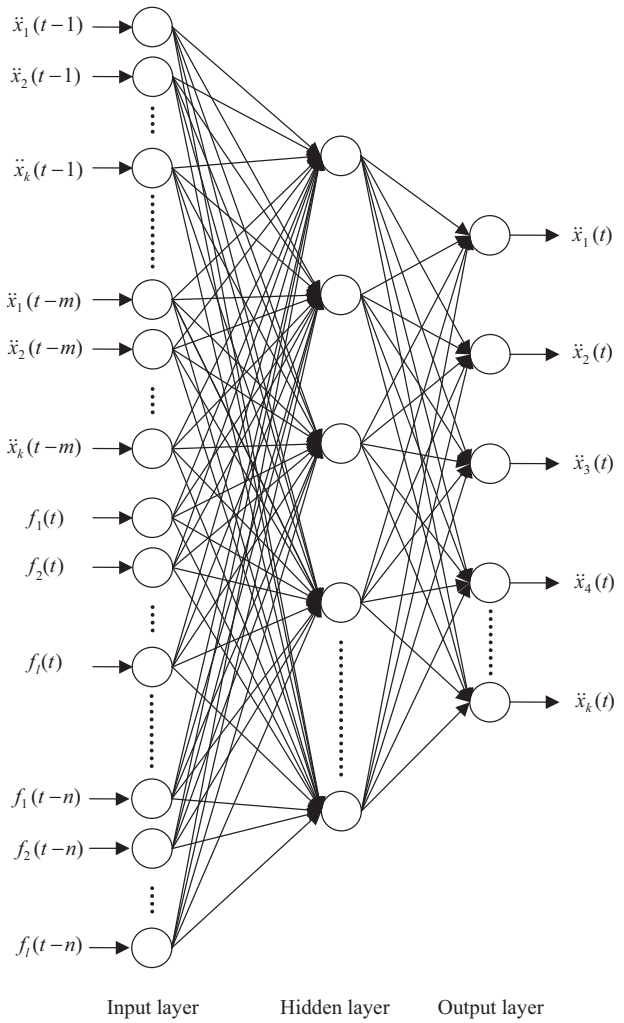

Figure 2. Topology of a neural network for modelling responses of a structure in earthquakes.

3.1. Construction of an ANN for a linear dynamic system

Acceleration responses are normally measured in monitoring the responses of a structure in an earthquake. Therefore, these measured data are used to train an ANN. Figure 2 illustrates the proposed architecture of the ANN, where $f_l(t-i)$, with $i=0,1,2,\ldots,n$, represents input base accelerations, corresponding to component l at $(t-i)$ time step, while $\ddot{x}_k(t-j)$, with $j=0,1,2,\ldots,m$, represents the observed acceleration responses of the kth degree of freedom relative to the base at the $(t-j)$ time step. Herein, a non-linear transfer function is used

and defined as,

$$g(y)=\begin{cases}1 & \text{when } y>1\\ y & \text{when } -1\leqslant y\leqslant 1\\ -1 & \text{when } y<-1\end{cases} \tag{17}$$

Notably, the values for nodes in the input layer are usually normalized to the range between 1 and -1 in training an ANN. Consequently, the argument of the transfer function is rarely larger than 1 or less than -1.

Following the procedure given earlier for establishing a BPN and using the observed responses of the target structure in a small earthquake, enables the connective weights and thresholds to be determined and an appropriate ANN to be established for the structural system.

3.2. Estimation of modal parameters

Careful investigation of the ANN established in the previous section reveals that the network yields a linear system if the transfer function is linear. The normalization of the values in the input nodes is such that the responses in the output layer are approximately related to the values of the input nodes by the following linear relationship.

$$\{Y\}=[W][V]\{X\}+([W]\{\theta_v\}+\{\theta_w\}) \tag{18}$$

where

$$\begin{aligned}\{Y\}&=(\ddot{x}_1(t),\ddot{x}_2(t),\ldots,\ddot{x}_k(t))^{\mathrm{T}},\quad \{X\}=(\bar{\mathbf{X}}\mathbf{F})^{\mathrm{T}}\\ \bar{\mathbf{X}}&=(\ddot{x}_1(t-1)\ddot{x}_2(t-1)\cdots\ddot{x}_k(t-1)\ddot{x}_1(t-2)\ddot{x}_2(t-2)\cdots\ddot{x}_k(t-2)\cdots\\ &\quad\ddot{x}_1(t-m)\ddot{x}_2(t-m)\cdots\ddot{x}_k(t-m))\\ \mathbf{F}&=(f_1(t)f_2(t)\cdots f_l(t)f_1(t-1)f_2(t-1)\cdots f_l(t-1)\cdots f_1(t-n)f_2(t-n)\cdots f_l(t-n))\end{aligned}$$

The elements of $[W]$ and $[V]$ are w_{ij} and v_{ij}, respectively, and the elements of $\{\theta_w\}$ and $\{\theta_v\}$ are θ_{wi} and θ_{vi}. Carefully expanding Equation (18) yields

$$\begin{Bmatrix}\ddot{x}_1(t)\\ \ddot{x}_2(t)\\ \vdots\\ \ddot{x}_k(t)\end{Bmatrix}=\sum_{i=1}^{m}\hat{\mathbf{W}}_1^{(i)}\begin{Bmatrix}\ddot{x}_1(t-i)\\ \ddot{x}_2(t-i)\\ \vdots\\ \ddot{x}_k(t-i)\end{Bmatrix}+\sum_{j=0}^{n}\hat{\mathbf{W}}_2^{(j)}\begin{Bmatrix}f_1(t-j)\\ f_2(t-j)\\ \vdots\\ f_l(t-j)\end{Bmatrix}+\{C\} \tag{19}$$

where

$$\begin{aligned}[\hat{\mathbf{W}}_1\ \ \hat{\mathbf{W}}_2]&=[W][V],\quad \{C\}=[W]\{\theta_v\}+\{\theta_w\},\quad \hat{\mathbf{W}}_1=[\hat{\mathbf{W}}_1^{(1)}\hat{\mathbf{W}}_1^{(2)}\cdots\hat{\mathbf{W}}_1^{(m)}]\\ \hat{\mathbf{W}}_2&=[\hat{\mathbf{W}}_2^{(0)}\hat{\mathbf{W}}_2^{(1)}\cdots\hat{\mathbf{W}}_2^{(n)}]\end{aligned}$$

Equation (19) is similar to the time-series model, ARX. The ARX model equates the equations of motion of a structural system. The dynamic characteristics of the system can be determined from the coefficient matrices of AR [15]. Constructing the matrix

$$[G] = \begin{bmatrix} 0 & \mathbf{I} & 0 & 0 & 0 \\ 0 & 0 & \mathbf{I} & 0 & 0 \\ \vdots & \vdots & \vdots & \vdots & \vdots \\ 0 & 0 & 0 & 0 & \mathbf{I} \\ \hat{\mathbf{W}}_1^{(m)} & \hat{\mathbf{W}}_1^{(m-1)} & \dots & \hat{\mathbf{W}}_1^{(2)} & \hat{\mathbf{W}}_1^{(1)} \end{bmatrix} \tag{20}$$

enables the modal parameters to be determined from the eigenvalues and eigenvectors of $[G]$ [16]. Let λ_k and $\{\psi_k\}$ represent the kth eigenvalue and eigenvector of $[G]$, respectively. The eigenvalue, λ_k, is normally a complex number, equal to $a_k + \mathrm{i}b_k$. The corresponding natural frequency and modal damping of the structural system are given by

$$\tilde{\gamma}_k = \sqrt{\sigma_k^2 + \gamma_k^2} \tag{21}$$

$$\xi_k = -\sigma_k / \tilde{\gamma}_k \tag{22}$$

where $\tilde{\gamma}_k$ is the pseudo-undamped circular natural frequency; ξ_k is the modal damping ratio;

$$\gamma_k = \frac{1}{\Delta t} \tan^{-1}\left(\frac{b_k}{a_k}\right) \tag{23}$$

$$\sigma_k = \frac{1}{2\Delta t} \ln(a_k^2 + b_k^2) \tag{24}$$

and $\frac{1}{\Delta t}$ is the sampling rate of measurement.

The special composition of $[G]$ in Equation (20) yields the following property of its eigenvectors:

$$\{\psi_k\} = (\{\psi_k\}_1^{\mathrm{T}}, \lambda_k\{\psi_k\}_1^{\mathrm{T}}, \lambda_k^2\{\psi_k\}_1^{\mathrm{T}}, \dots, \lambda_k^{m-1}\{\psi_k\}_1^{\mathrm{T}})^{\mathrm{T}} \tag{25}$$

where $\{\psi_k\}_1$ is the complex modal shape of the system, corresponding to the natural frequency, $\tilde{\gamma}_k$.

Notably, the formulation shown above is easily extended to cases with multiple hidden layers, by modifying only the definitions for $\hat{\mathbf{W}}_1^{(i)}$, $\hat{\mathbf{W}}_2^{(j)}$ and $\{C\}$ in Equation (19).

Various ANNS with the architecture given in Figure 2, can be established, from the measured responses of a structure in earthquakes with various magnitudes. The modal parameters for the structure in different earthquakes can be determined from the established ANNs, by the above approach. Considerable changes in modal parameters, corresponding to different ANNs, indicate significant changes in the properties of the structure in different earthquakes.

An index commonly used to evaluate the correlation of modal shapes obtained from different ANNs, is based on the modal assurance criterion (MAC) [17] defined as

$$\mathrm{MAC}(\boldsymbol{\varphi}_{\mathrm{iR}}, \boldsymbol{\varphi}_{\mathrm{iC}}) = \frac{|\boldsymbol{\varphi}_{iR}^{\mathrm{T}} \boldsymbol{\varphi}_{\mathrm{iC}}^{*}|^2}{\boldsymbol{\varphi}_{\mathrm{iR}}^{\mathrm{T}} \boldsymbol{\varphi}_{\mathrm{iR}}^{*} \boldsymbol{\varphi}_{\mathrm{iC}}^{\mathrm{T}} \boldsymbol{\varphi}_{\mathrm{iC}}^{*}} \tag{26}$$

where * denotes the complex conjugate, $\boldsymbol{\varphi}_{iR}$ and $\boldsymbol{\varphi}_{iC}$ represent the ith complex mode shapes for the reference state and the current state to which it is to be compared, respectively. Apparently, two corresponding modes are highly correlated if the MAC value is close to one, and uncorrelated if it is near zero.

As shown in the following section, the MAC value is not very sensitive to the changes in modal shapes for the cases considered here. Thus, an index proposed by Trifunac [18] for modal shapes in a proportional damping system, is adopted here. The index is defined as

$$e = \left(\frac{(\boldsymbol{\varphi}_{iR} - a\boldsymbol{\varphi}_{iC})^{T}(\boldsymbol{\varphi}_{iR} - a\boldsymbol{\varphi}_{iC})^{*}}{\boldsymbol{\varphi}_{iR}^{T}\boldsymbol{\varphi}_{iR}^{*}} \right)^{1/2} \tag{27}$$

where the complex constant, a, is obtained by minimizing $(\boldsymbol{\varphi}_{iR} - a\boldsymbol{\varphi}_{iC})^{T}(\boldsymbol{\varphi}_{iR} - a\boldsymbol{\varphi}_{iC})^{*}$. Equation (27) reveals that e is close to zero when the two modal shapes are highly correlated.

3.3. Prediction error in responses from the established ANN

The ANN established for a linear structural system is expected to be able to predict accurately the current responses, from previously measured responses and inputs, if the structural system remains linear and the modal properties do not significantly change. However, when the structural system is damaged or has deteriorated, it will exhibit non-linear behaviour resulting in a large error in the responses of this damaged structure, predicted by the ANN trained for the healthy, linear structure. The indexes proposed by Masri *et al.* can be used to quantify this error. [10] However, for simplicity, only the mean absolute error (MAE) between the output predicted by the trained ANN, and the measured acceleration responses is computed for each degree of freedom, and is defined as

$$\mathrm{MAE}(i) = \frac{1}{T}\sum_{t=1}^{T} |y_{im}(t) - y_{ip}(t)| \tag{28}$$

where i represents the ith degree of freedom, and y_{im} and y_{ip} are the normalized measurements and the predicted responses for the ith degree of freedom, respectively. Notably, throughout this paper, the measurements for various base excitations were independently normalized such that the maximum responses were normalized to 0.9.

4. APPLICATION TO A FRAME IN SHAKING TABLE TESTS

Shaking table tests are often performed in a laboratory to examine the behaviour of structures in earthquakes. The National Center for Research in Earthquake Engineering in Taiwan undertook a series of shaking table tests on a 3 m long, 2 m wide, and 6.5 m high steel frame [19] (Figure 3) to generate a set of earthquake response data for this benchmark model of a five-storey steel structure. Lead blocks were piled on each floor such that the mass of each floor was approximately 3664 kg. The frames were subjected to the base excitation of the Kobe earthquake, weakened by various levels. The displacement, velocity and acceleration response histories of each floor were recorded during the shaking table tests. Additionally, some strain gauges were also installed in one of the columns and near the first floor. The sampling rate of the raw data was 1000 Hz. These raw data were reproduced with a 200 Hz

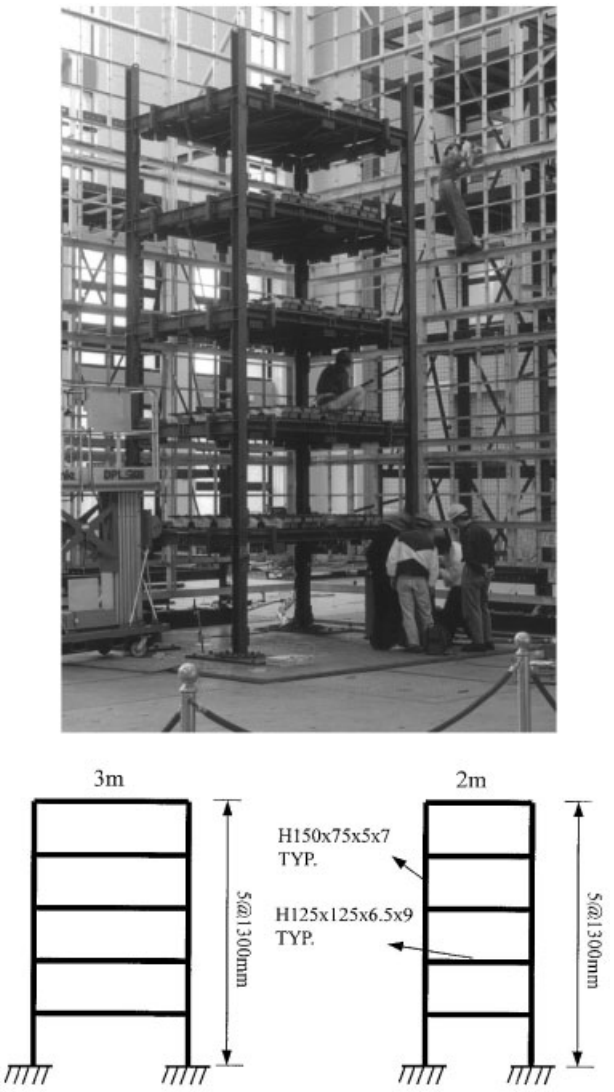

Figure 3. A photo and simple sketch of a five-storey steel frame.

sampling rate by taking one data point out of every five raw data points to save computational time and to match to the typical sampling rate for real applications.

Notably, it was reported [19] that the frame responded linearly when it subjected to 8, 10, 20, 40, and 52% of the strength of the Kobe earthquake. Measured strains and visual inspection revealed that 60% of the strength of the Kobe earthquake input caused the steel columns near the first floor to yield. In the following, only the responses and inputs in the long span direction are discussed.

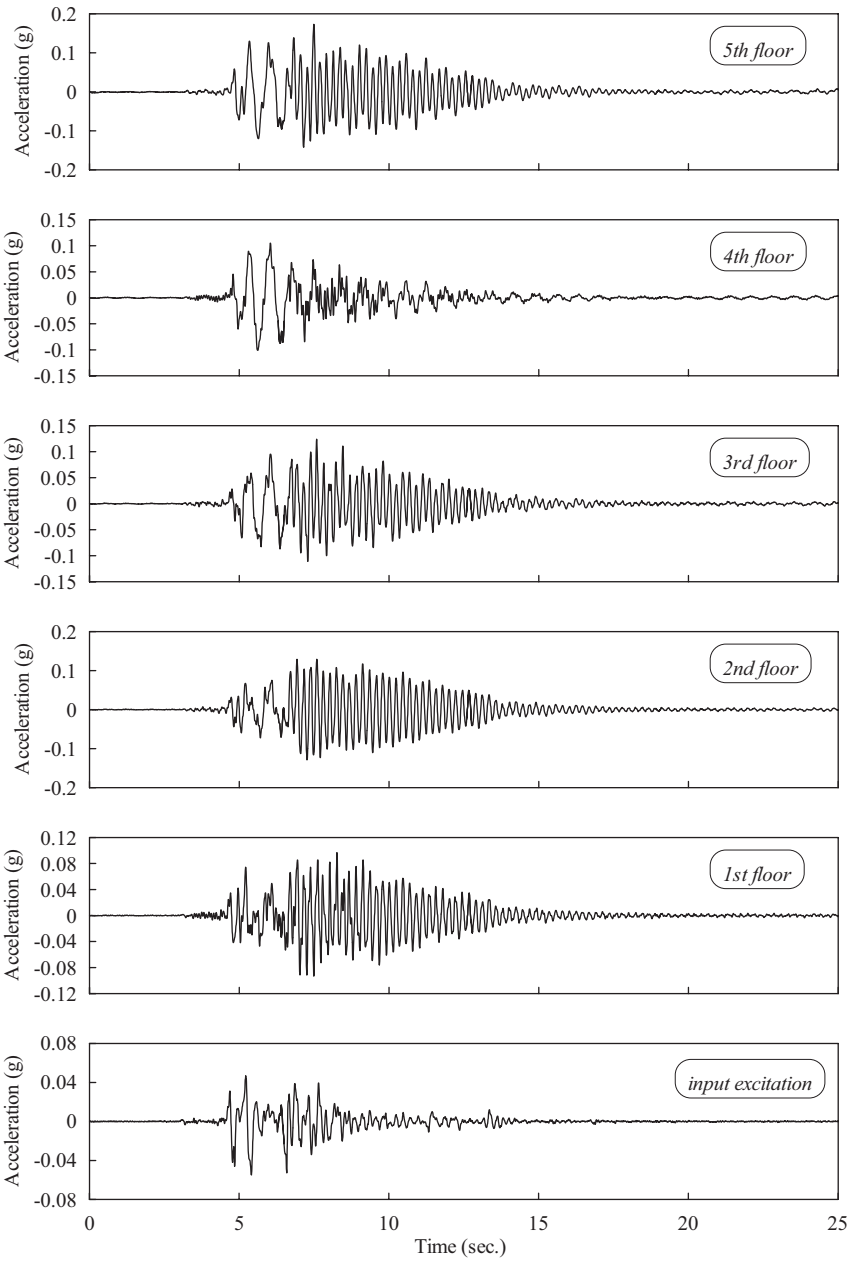

Figure 4. Response histories for 8% Kobe earthquake input.

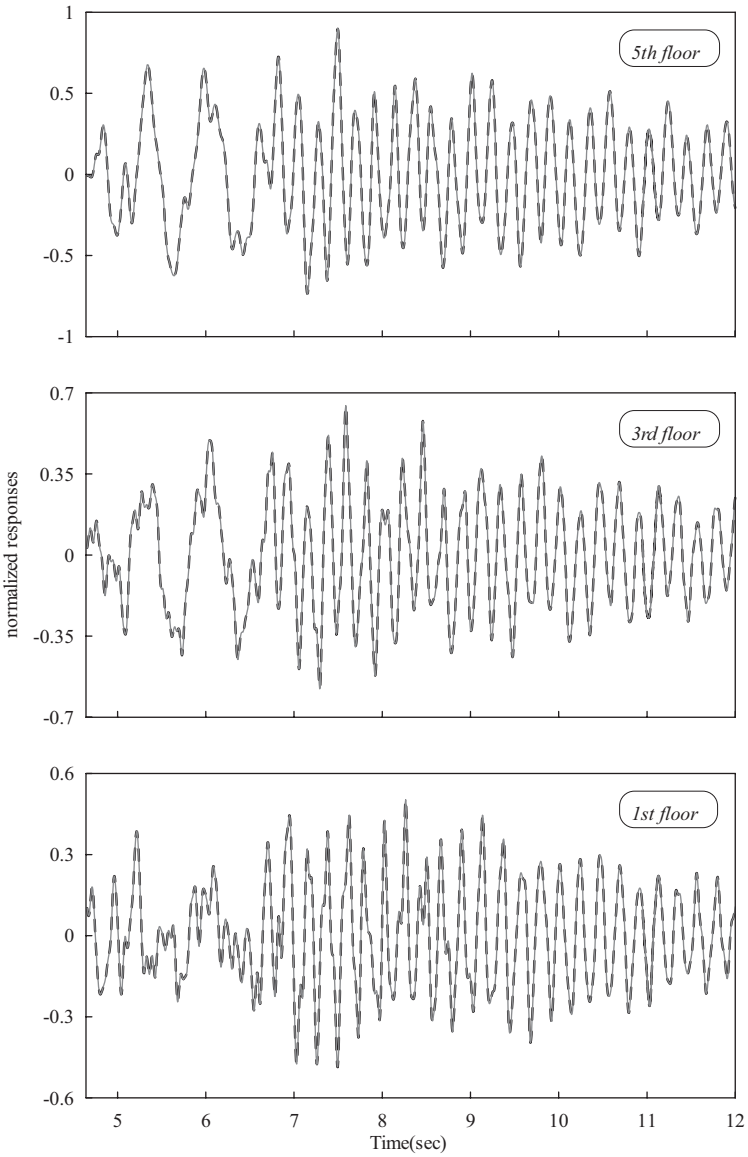

Figure 5. Comparison between the measured (solid line) and predicted (dash line) responses for 8% Kobe earthquake input.

4.1. Examination of the frame at 8% of the strength of the Kobe earthquake

Figure 4 depicts time histories of the acceleration responses of each floor, when the steel frame was subjected to 8% of the strength of the Kobe earthquake. The steel frame responded linearly at this level. The large responses between 4.5 and 12.5 s were used to train an ANN

Table I. Comparison of the identified modal parameters for 8% Kobe earthquake input.

Method	Mode	Frequency (Hz)	Damping (%)	MAC	e (%)
Present	1	1.40	1.56	1.00	0.38
	2	4.53	0.17	1.00	0.15
	3	8.23	0.17	1.00	0.31
	4	12.39	0.13	1.00	0.47
	5	15.99	0.11	1.00	0.47
Subspace	1	1.40	1.30	/	/
	2	4.53	0.16	/	/
	3	8.23	0.19	/	/
	4	12.39	0.13	/	/
	5	15.99	0.10	/	/

Note: /: no data available.

and thus, to some extent, reduce the noise effect. The architecture of the ANN is as shown in Figure 2, with $k = 5$, $l = 1$, $m = n = 30$ and ten nodes in the hidden layer. This architecture was used throughout this paper. The acceleration responses of each floor relative to the base were used to train an ANN. Figure 5 shows the excellent correspondence between the observed responses and the computed responses from the trained ANN for the 1st, 3rd, and 5th floors. It is noted that the computed responses in Figure 5 were obtained from the trained ANN by using the observed data as input of the ANN.

Table I lists the identified modal parameters obtained from the trained ANN, which excellently agree with those obtained by Huang and Lin [20] who used a subspace technique to process the same response data. This consistency confirms the correctness of the proposed procedure of determining the modal parameters from an ANN.

4.2. Examination of the frame in the Kobe earthquake with various reduction levels

The measured acceleration responses of the frame under the base excitations with various reduction levels of the Kobe earthquake, enables the corresponding ANNs to be established and the corresponding modal parameters to be determined. Table II summarizes the results, in which the values, MAC and e, designate the correlation between the modal shapes for an input of 20% Kobe earthquake and those for inputs with other reduction levels.

Table II reveals that the frequencies for each mode generally decrease as the excitation magnitude increases, but the changes in frequency are quite small. Generally, the modal damping values increase with excitation magnitude. The modal damping values for the 60% Kobe earthquake are much greater than those for the 10% Kobe. Interestingly, only the damping for the first mode exceeds 1% while the damping for the other modes is typically much less than 1%. The MAC values in Table II indicate that the modal shapes for the 20% Kobe earthquake are likely to correlate closely with those for other excitations. However, e values clearly show that the modal shapes of the higher modes (3–5th) for the 60% Kobe earthquake notably differ from those for the 20% Kobe earthquake, since the corresponding e values exceed 10%. Apparently, the e values are more sensitive to the differences in modal shapes than the MAC values. The damping and e values truly reflect the fact of possible damage of the frame under the 60% Kobe earthquake input.

Table II. Identified modal parameters for different inputs.

Excitation	Mode	Frequency (Hz)	Damping (%)	MAC	e (%)
	1	1.40	1.65	1.00	1.00
	2	4.53	0.18	1.00	0.59
10% Kobe	3	8.24	0.22	1.00	0.66
	4	12.38	0.16	1.00	0.79
	5	16.00	0.16	1.00	1.17
	1	1.39	1.73	/	/
	2	4.53	0.25	/	/
20% Kobe	3	8.23	0.28	/	/
	4	12.37	0.18	/	/
	5	15.97	0.15	/	/
	1	1.38	2.42	1.00	0.65
	2	4.50	0.47	1.00	0.92
40% Kobe	3	8.18	0.19	1.00	2.26
	4	12.36	0.21	1.00	6.58
	5	15.93	0.07	1.00	4.54
	1	1.37	2.89	1.00	0.42
	2	4.49	0.69	1.00	1.13
52% Kobe	3	8.14	0.53	1.00	3.36
	4	12.33	0.15	1.00	5.48
	5	15.91	0.58	1.00	6.83
	1	1.35	3.73	1.00	2.21
	2	4.45	0.92	1.00	5.24
60% Kobe	3	8.07	0.84	0.99	11.52
	4	12.24	0.83	0.98	13.42
	5	15.88	0.26	0.98	13.13

Note: /: no data available.

4.3. Identifying modal parameters from windowed responses

Although using more data to train an ANN yields a more accurate network, it is interesting to investigate the changes in modal parameters identified from different portions of response records. The responses from $t = 4.5$ to 12.5 s were divided into nine segments, each of 4 s, each of which overlays 3.5 s of the previous one. Table III presents the modal parameters, identified by ANNs trained with different segments of data for the 20 and 60% Kobe earthquakes. Notably, the e values for the first segment were computed with reference to the modal shapes obtained using the responses between $t = 4.5$ and 12.5 s, while the e values for other segments refer to the modal shapes for the first segment.

Table III shows that using different segments of data leads to no significant variation in the identified frequencies. These frequencies are substantially consistent with those in Table II, obtained by using the entire response. The damping values do differ somewhat with different segments of data, perhaps because the damping matrix in the equations of motion is artificially defined, such that the damping coefficients for a real structure may change as it vibrates. Interestingly, the modal shapes obtained from different segments for the 20% Kobe

earthquake input show no significant differences. However, considerable differences in higher modal shapes are observed for different segments in the 60% Kobe earthquake input, indicating non-linear responses in this case.

4.4. Prediction error of the trained ANN

The responses at a moderate reduction level (say, 20%) of the Kobe earthquake input were selected to establish the ANN to predict the responses to other inputs. Figure 6 shows an excellent agreement between the observed responses and the computed responses from the trained ANN for the 1st, 3rd and 5th floors subjected to the 20% Kobe earthquake input. Figure 7 compares the measured and predicted responses for the 60% Kobe earthquake input. Notably, the observed data were used as input of the trained ANN to obtain the computed responses in Figures 6 and 7. Comparing Figures 6 and 7 reveals that the discrepancies between prediction and measurement for the 60% Kobe earthquake input far exceed those for the 20% Kobe earthquake input. Figure 7 shows that there are high frequency responses between $t = 5.5$ and 6.5 s, which lead to large prediction errors. It should be mentioned that the responses in Figures 6 and 7 were normalized according to the maximum responses in each figure, respectively.

The MAE values of each floor for various reduction levels of the Kobe earthquake are divided by the MAE value for the 20% Kobe earthquake and presented in Figure 8. The small changes in the modal parameters for the frame with different inputs, discussed in the earlier sections, cause the prediction errors to increase for the 10, 40 and 52% Kobe earthquake inputs. The relative MAE values for the responses to the 60% Kobe earthquake input greatly exceed the other relative MAE values, confirming the reported non-linear responses to the 60% Kobe earthquake input [17]. Further investigation is required to determine whether the larger relative MAE values for the first and second floors in the 60% Kobe earthquake input follow from the yielding of the columns near the first floor.

5. CONCLUDING REMARKS

This work has presented a novel procedure for diagnosing a structure from its earthquake acceleration responses, using an ANN model. The diagnosis is based on the fact that damage to a structure induces non-linear structural responses to earthquakes and considerably changes both the modal parameters of an equivalent linear system and the output errors predicted by a neural network trained for the structure without any damage. The modal parameters are directly estimated from the weighting matrices in the ANN model. The output prediction errors for each measured degree of freedom of the structure are determined from the measured responses to various earthquakes, and the corresponding prediction of the ANN model trained by data for a small earthquake.

The proposed method of estimating the modal parameters has been verified by excellent agreement between the present results and those results obtained by a subspace method, for a five-storey steel frame under base excitation in a shaking table test. The proposed diagnosis procedure has also been applied to the acceleration responses of the steel frame under base excitations with different reduction levels of the Kobe earthquake in shaking table tests.

Table III. Identified modal parameters from windowed responses.

Excitation	Parameter	Mode	Segment									Mean (μ)	STD# (σ)	σ/μ
			1	2	3	4	5	6	7	8	9			
		1	1.39	1.39	1.39	1.39	1.39	1.40	1.40	1.40	1.40	1.40	0.0050	0.0036
		2	4.53	4.53	4.53	4.53	4.53	4.53	4.53	4.53	4.53	4.53	0	0
	Frequency (Hz)	3	8.23	8.23	8.23	8.23	8.23	8.23	8.23	8.23	8.23	8.23	0	0
		4	12.37	12.37	12.38	12.38	12.38	12.38	12.38	12.38	12.38	12.38	0.0042	0.0003
		5	15.97	15.96	15.97	15.97	15.98	15.97	15.99	15.98	15.98	15.97	0.0083	0.0005
		1	1.76	1.80	1.57	1.22	0.92	1.16	1.48	1.39	1.32	1.40	0.27	0.19
		2	0.27	0.28	0.27	0.27	0.26	0.23	0.18	0.19	0.18	0.24	0.04	0.17
20%	Damping (%)	3	0.29	0.30	0.28	0.26	0.28	0.24	0.23	0.15	0.23	0.25	0.14	0.17
		4	0.21	0.20	0.20	0.19	0.18	0.20	0.15	0.15	0.11	0.18	0.03	0.18
		5	0.16	0.17	0.11	0.08	0.10	0.03	0.12	0.10	0.09	0.11	0.04	0.37
		1	0.07*	0.05	0.08	0.13	0.24	0.25	0.38	0.43	0.52	0.26	0.16	0.62
		2	0.15*	0.05	0.06	0.12	0.16	0.18	0.56	0.57	0.54	0.28	0.22	0.78
	e (%)	3	0.15*	0.02	0.24	0.29	0.28	0.48	0.66	0.63	0.56	0.42	0.17	0.42
		4	0.56*	0.49	0.38	0.56	0.74	1.02	0.99	1.47	1.45	0.89	0.39	0.44
		5	0.42*	0.48	1.05	0.93	0.82	2.47	2.27	1.84	2.27	1.52	0.73	0.48
		1	1.35	1.35	1.35	1.35	1.35	1.35	1.35	1.35	1.37	1.36	0.0068	0.0051
		2	4.44	4.43	4.44	4.44	4.44	4.46	4.48	4.47	4.48	4.45	0.0183	0.0041
	Frequency (Hz)	3	8.05	8.04	8.03	8.06	8.06	8.07	8.13	8.16	8.22	8.09	0.0608	0.0075
		4	12.24	12.23	12.24	12.25	12.25	12.26	12.25	12.26	12.28	12.25	0.0137	0.0011
		5	15.88	15.88	15.88	15.88	15.88	15.89	15.89	15.90	15.88	15.88	0.0068	0.0004
		1	4.11	3.99	4.04	3.57	3.33	3.07	2.90	2.91	2.75	3.41	0.51	0.15
		2	1.00	1.05	1.04	1.05	0.98	0.95	0.67	0.50	0.42	0.85	0.24	0.28
60%	Damping (%)	3	0.69	0.77	0.73	0.90	1.01	1.66	0.86	1.04	0.53	0.91	0.30	0.34
		4	0.91	0.89	0.86	0.88	0.81	0.70	0.56	0.68	0.57	0.76	0.13	0.17
		5	0.23	0.19	0.15	0.17	0.18	0.16	0.16	0.33	0.29	0.21	0.06	0.29
		1	0.85	0.78	0.79	0.51	0.54	1.32	1.46	1.44	1.58	1.05	0.41	0.39
		2	1.04*	0.57	0.39	0.39	0.82	2.46	3.50	3.74	4.09	2.00	1.52	0.76
	e (%)	3	1.83*	1.62	3.12	4.58	2.97	4.86	8.11	7.87	7.35	5.06	2.31	0.46
		4	1.68*	1.35	0.99	3.01	1.55	6.10	5.95	3.13	7.21	3.66	2.28	0.62
		5	11.48*	5.81	6.11	8.16	7.22	9.88	18.14	23.68	28.98	13.50	8.36	0.62

Note: $*$: Referring to modal shapes obtained by using the responses from $t = 4.5$ to 12.5 s. #: Standard deviation.

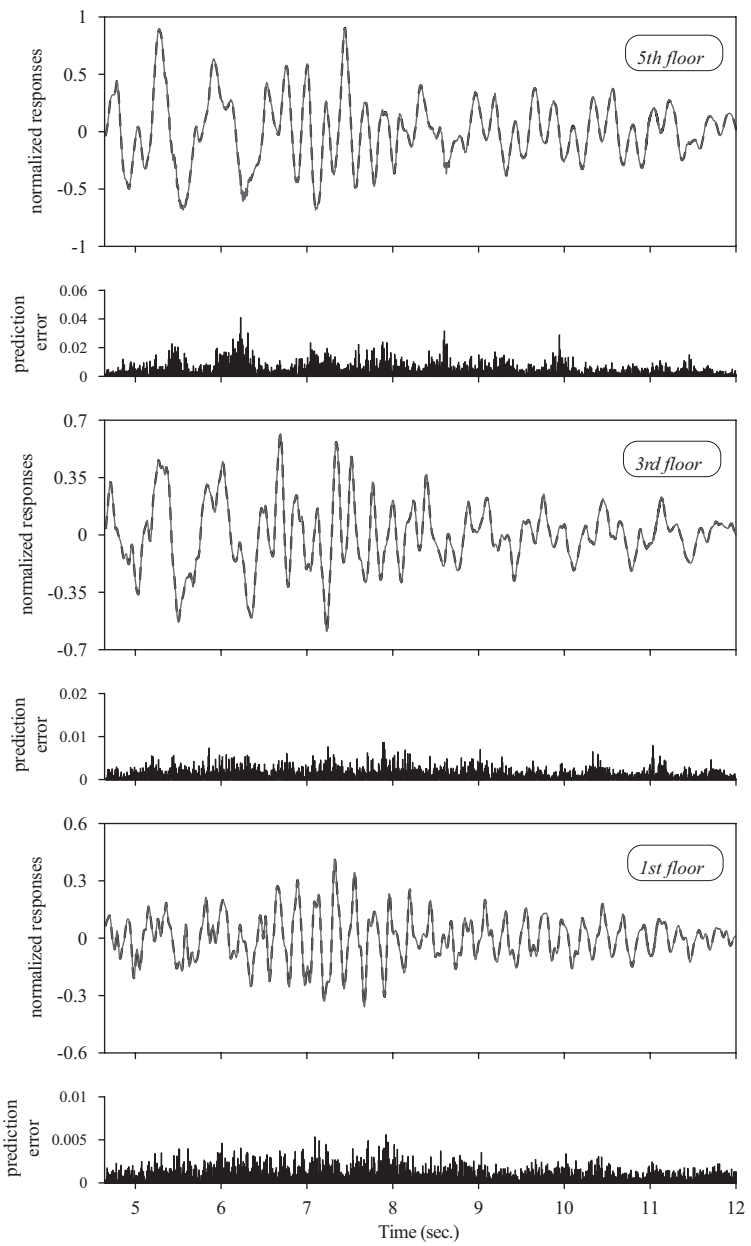

Figure 6. Comparison of the measured (solid line) and predicted (dash line) responses for 20% Kobe earthquake input.

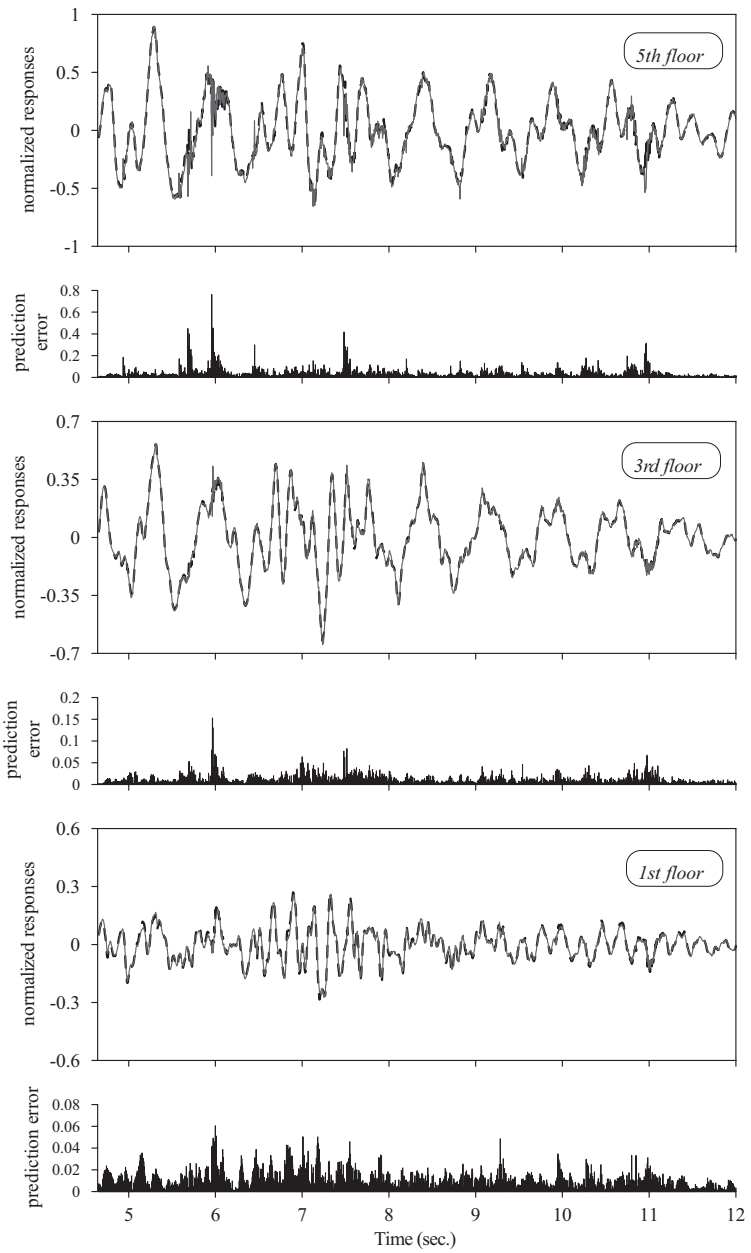

Figure 7. Comparison of the measured (solid line) and predicted (dash line) responses for 60% Kobe earthquake input.

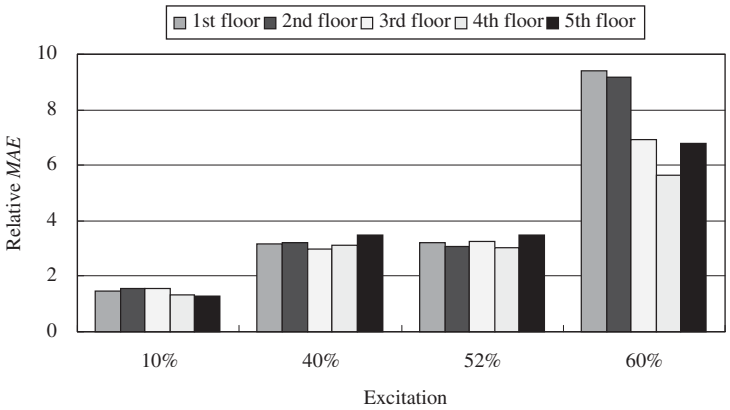

Figure 8. Relative mean absolute errors of predictions for the Kobe earthquake inputs with various reduction levels.

The reported non-linear responses to the 60% Kobe earthquake input were found to change significantly modal shapes and damping values from those for the frame in the 20% Kobe earthquake input. Considerable prediction errors were also found when the ANN model, trained with responses to the 20% Kobe earthquake input, was used to predict the responses to the 60% Kobe earthquake input. However, no significant changes were found in the modal parameters obtained from the responses for the 8, 10, 20, 40, and 52% Kobe earthquake inputs that caused no damage to the frame. The prediction errors of the ANN, trained using the responses to the 20% Kobe earthquake, for the responses to the 10, 40 and 52% Kobe earthquake inputs were much smaller than that for the 60% Kobe earthquake input responses. These results show the applicability of the proposed procedure in diagnosing whether a structure is healthy.

Future work should apply the proposed approach to measurements in the field to show (or even improve) its capacity to process possibly incomplete measurements, substantially corrupted by noise. Moreover, the ability of the proposed approach to detect the location of damage should also be further verified or improved.

ACKNOWLEDGEMENTS

This work reported herein was supported by the National Science Council, R.O.C. through research grant no. NSC90-2211-E-009-031. This support is gratefully acknowledged. The appreciation is also extended to the National Center for Research on Earthquake Engineering for providing shaking table testing data.

REFERENCES

1. Hearn G, Testa RB. Modal analysis for damage detection in structures. *Journal of Structural Engineering* (ASCE) 1991; **117**(10):3042–3063.
2. Alampalli S, Fu GK. Full scale dynamic monitoring of highway bridges. *Structural Engineering in Natural Hazards Mitigation*, vol. 1, 1993; 1602–1607.

3. Salawu OS, Williams C. Bridge assessment using forced-vibration testing. *Journal of Structural Engineering* (ASCE) 1995; **121**(2):161–173.
4. Koh CG, See LM, Balenra T. Damage detection of buildings: Numerical and experimental studies. *Journal of Structural Engineering* (ASCE) 1995; **121**(8):1155–1160.
5. Wu X, Ghaboussi J, Garrett JH. Use of neural networks in detection of structural damage. *Computers and Structures*, 1992; **42**(4):649–659.
6. Elkordy MF, Chang KC, Lee GC. Neural networks trained by analytically simulated damage states. *Journal of Computing in Civil Engineering* (ASCE) 1993; **7**(2):130–145.
7. Szewczyk ZP, Hajela P. Damage detection in structures based on feature-sensitive neural network. *Journal of Computing in Civil Engineering* (ASCE) 1994; **8**(2):163–178.
8. Pandey PC, Barai SV. Multilayer perceptron in damage detection of bridge structures. *Computers and Structures* 1995; **54**(4):597–608.
9. Zhao J, Ivan JN, DeWolf JT. Structural damage detection using artificial neural networks. *Journal of Infrastructure Systems* (ASCE) 1998; **4**(3):93–101.
10. Masri SF, Smyth AW, Chassiakos AG, Caughey TK, Hunter NF. Application of neural networks for detection of changes in nonlinear systems. *Journal of Engineering Mechanics* (ASCE) 2000; **126**(7):666–676.
11. Rumelhart DE, Hinton GE, Williams RJ. Learning international representation by error propagation. In *Parallel Distributed Processing*, Rumelhart DE, *et al.* (eds). The MIT Press: Cambridge, MA, 1986; 318–362.
12. Hecht-Nielsen R. Theory of the back propagation neural network. *Proceedings of International Joint Conference on Neural Networks*. IEEE: New York, 1989; **1**:593–605.
13. Hung SL, Lin YL. application of an L-BFGS neural network learning algorithm in engineering analysis and design. *Proceedings of the 2nd National Conference on Structural Engineering*. Chinese Society of Structural Engineering: Taiwan, R.O.C., 1994 (in Chinese).
14. Nocedal J. Updating quasi-Newton matrix with limited storage. *Mathematics of Computation* 1980; **35**:20–33.
15. Huang CS. Structural identification from ambient vibration measurement using the multivariate AR model. *Journal of Sound and Vibration* 2001; **241**(3):337–359.
16. Huang CS. A study on techniques for analyzing ambient vibration measurement (II)-time series methods. Report No. NCREE-99-018, *National Center for Research on Earthquake Engineering*. R. O. C., 1999 (in Chinese).
17. Allemang RL, Brown DL. A correlation coefficient for modal vector analysis. *Proceedings of the first International Model Analysis Conference*, Bethel, Connecticut, U.S.A., 1983; 110–116.
18. Trifunac D. Comparisons between ambient and forced vibration experiments. *Earthquake Engineering and Structural Dynamics* 1972; **1**:133–150.
19. Yeh SC, Cheng CP, Loh CH. Shaking table tests on scaled down five-story steel structures. *NCREE Report No. NCREE*-99-002, *National Center for Research on Earthquake Engineering*, R.O.C., 1999 (in Chinese).
20. Huang CS, Lin HL. Modal identification of structures from ambient vibration, free vibration, and seismic response data via a subspace approach. *Earthquake Engineering and Structural Dynamics* 2001; 30:1857–1878.

